Cement and Concrete Composites 75 (2017) 1–9

Contents lists available at ScienceDirect

Cement and Concrete Composites

journal homepage: www.elsevier.com/locate/cemconcomp

A pore water pressure diffusion model to predict formwork pressure exerted by freshly mixed concrete

Chan Kyu Park [a], Jae Hong Kim [b, *], Seong Ho Han [b]

[a] Institute of Construction Technology, Samsung Corporation, Seoul, Republic of Korea
[b] School of Urban and Environmental Engineering, Ulsan National Institute of Science and Technology, Republic of Korea

ARTICLE INFO

Article history:
Received 21 August 2015
Received in revised form
15 June 2016
Accepted 28 September 2016
Available online 29 September 2016

Keywords:
Bleeding
Formwork pressure
Fresh concrete
Rheology
Diffusion

ABSTRACT

The formwork pressure exerted by freshly mixed concrete is one of the most important considerations in ensuring the safety of construction in the field. The formwork pressure also affects the quality of concrete structures, determining the final shape of concrete members. Previous studies on the form pressure mostly investigated the intrinsic material effect. For example, the use of self-consolidating concrete increases the maximum pressure on the formwork. The extrinsic factor of a formwork system itself has rarely been considered. In the mockup tests and theoretical evaluations, it is identified that the bleed water-out controlled by the formwork tightness is critical. A pore water pressure diffusion model consistently addresses the high form pressure exerted by self-consolidating concrete, showing little bleeding, or by normally vibrated concrete placed in a waterproofed formwork.

1. Introduction

Accidents in the process of concrete placement reportedly cause heavy casualties during the construction of concrete structures. For example, two major accidents in Korea were reported in 2015. Each case led to approximately 10 laborer casualties. These accidents were triggered by the collapse of a roof-slab form or bridge-deck form when the concrete was placed. Questions are being asked regarding the safety of form and shoring systems. The formwork pressure exerted by freshly mixed concrete is one of the most important considerations in the design of form and shoring systems.

Introducing cast-in-place self-consolidating concrete (SCC) has led to quantitative evaluations and analyses of the form pressure since the early 2000s. The conventional formula for the form pressure, such as the ACI 327 guideline for formwork [1,2], hardly considers the fluidity of self-consolidating concrete. A higher level of form pressure load was then proposed for self-consolidating concrete in the DIN code [3], where the placement rate was revealed as the most influential parameter [4,5]. The current update reflected a variety of experimental measurement on the form pressure exerted by SCC [6–8]. Understanding the lateral pressure response and its decay was accomplished with several models such as a phenomenological model based on the pressure response [9–11], the increase of thixotropic resistance [12–14], or pore water pressure [15,16]. The hypotheses on intrinsic effect of freshly mixed concrete could be categorized as follows: (1) the cohesion-friction model, such as the Mohr-Coulomb theory and Rowe's theory [17,18]; (2) the rheological evaluation based on the thixotropic evolution of the yield stress [19,20]; and (3) decay of the pore water pressure in cement-based materials [21–23]. Still, the mechanism of form pressure decay requires additional study.

On the other hand, the previously described accidents also indicate the effect of formwork materials, an extrinsic factor. The old-fashioned wood gang-form has been replaced by steel or polymeric composite system-forms for the efficiency of formwork installation in construction sites. Note that the conventional ACI formula was based on the traditional formwork. The change of formwork material affects the form pressure. A limited number of studies reported the evaluation of the effect of the form friction [24,25]. The variance on form pressure was also recorded according to the form surface material [26].

In these days, the efficient system-form composed of polymeric composites or steel isolates the freshly placed concrete inside it and almost flawlessly prevents the leakage of bleed water. The bleed-waterproofed form system presumably causes excess pore water

* Corresponding author.
E-mail address: jaekim@unist.ac.kr (J.H. Kim).

http://dx.doi.org/10.1016/j.cemconcomp.2016.09.009
0958-9465/

pressure on freshly mixed concrete, which results in a higher form pressure. The diffusion of pore water pressure in freshly mixed concrete addresses the decay of form pressure. In this study, a comprehensive model based on decay of the pore water pressure is proposed to analyze the effect of formwork materials. Applying the Biot theory of poroelasticity allows us to formulate the diffusion of pore water pressure and then predict the form pressure exerted by the freshly mixed concrete. Both normally vibrated concrete (NVC) and SCC were consistently evaluated under the same formulation. A mockup test considering a 3.4-m high column were performed to verify the proposed model.

2. Materials and methods

2.1. Sample preparation

Two concrete samples were produced by a local ready-mixed concrete supplier. Both samples were frequently adopted in the field and verified as having no difficulty in quality assurance. One sample was an NVC proportioned with a water-to-binder ratio (w/b) of 0.52; its nominal strength was 24 MPa, and its slump was 150 mm. The other sample was an SCC proportioned with a w/b of 0.35, which resulted in a nominal strength higher than 50 MPa; its slump flow was 700 mm. Table 1 reports the mix proportions of both samples, where GGBFS is ground-granulated blast-furnace slag and HRWRA is a polycarboxylate-based high-range water-reducing admixture.

Two mockup formworks were also assembled to compare the effect of bleeding leakage. These mockups had the same dimensions to eliminate the size effect on the form pressure. The height of each mockup was designed to contain a 3.4-m concrete head, and the cross section was 500 mm by 500 mm. Fig. 1 shows the dimensions of the two formworks. The shape of the formwork was a 4-sided pipe composed of 5-mm thick plates. Each plate was stiffened by ribs at intervals of 300 mm. Bolts with nuts were fastened between each of the side-plates. Therefore, it can be said that the formwork is stiff enough to disregard any deformation during the placement of concrete. The use of rubber pad and duct tape waterproofed edges of the 4 steel side-plates resulted in no water leaking out in the lateral direction of the form plates. Therefore, the two forms control the bleed water flow within the vertical direction: to the top or to the bottom.

The leakage of bleed water, the experimental variable in this study, was defined by the boundary condition of the forms. One formwork sample was stood up on a hardened concrete block. The form, a 4-sided pipe having no bottom cover, was anchored in the concrete block. The installation on the concrete block corresponds to a construction joint in the field, which allowed for water bleed-out (leakage) at the interface between the form and concrete block. The boundary condition at the bottom allowed limited perviousness. The other formwork sample, by contrast, was closed with a bottom cover. No water was allowed to come out at the bottom. Bleeding of concrete was allowed through its top surface only. Other factors affecting the form pressure were controlled to not govern the result of the experiment. For example, no reinforcement was considered on the samples. Note that the high ratio of reinforcement reportedly decreases the form pressure [27].

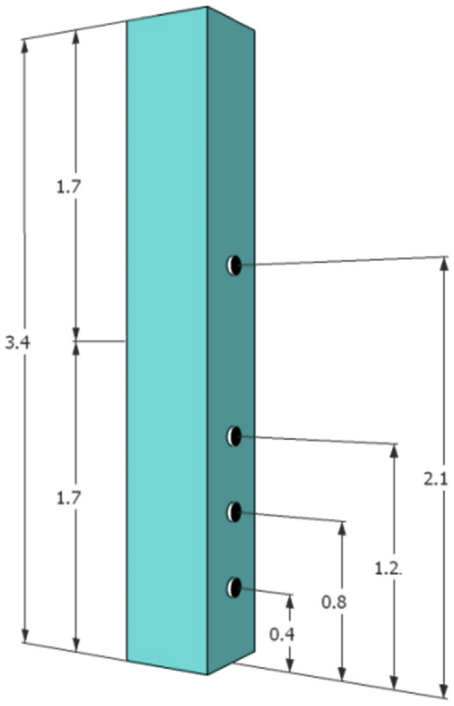

Fig. 1. Dimension of the formwork and the locations of pressure transducers. The unit of length is meter.

Table 2
Mockup test samples.

Case	Boundary condition	Placement execution
NVC0	Waterproofed	2-step placement
NVC1	Form on the concrete block	Single step placement
NVC2	Form on the concrete block	2-step placement
SCC2	Form on the concrete block	2-step placement

A total of 4 samples were tested and analyzed; these samples are labeled NVC0, NVC1, NVC2 and SCC2 in Table 2. The first 3 samples used normally vibrated concrete, showing a slump of 150 mm. The last sample adopted SCC, showing a slump flow of 700 mm. The last digit '0' on the labels indicates the use of the waterproofed form (with bottom cover). The digit of '1' or '2' indicates the placement plan with the use of a hopper: single step placement up to the top of the form (3.4 m concrete head) vs. 2-step placement with an interval of 1 h (double of 1.7 m concrete head). Fig. 2 shows a picture of the placement. During the placement and the subsequent pressure measurement, the air temperature was controlled in the range of 12 °C to 14 °C, and the temperature on the form surface increased up to approximately 17 °C for 5 h. Both NVC and SCC samples show the same pattern of temperature rise during the given period.

A total of 4 pressure transducers were installed, each of which had direct contact with the concrete. A hole was made on the form plate. A flush diaphragm pressure transducer that had a capacity of 13.8 bar was fit into the hole; its measuring surface was covered

Table 1
Mix proportion of concrete samples.

Sample	Water	Cement	Fly ash	GGBFS	Sand	Coarse sand	Gravel	HRWRA
NVC	176	205	51	85	248	579	917	2.39
SCC	166	379	–	95	392	391	933	6.64

§ The units are kg for producing 1 m^3 concrete.

Fig. 2. Picture of placing process of the mockup test samples.

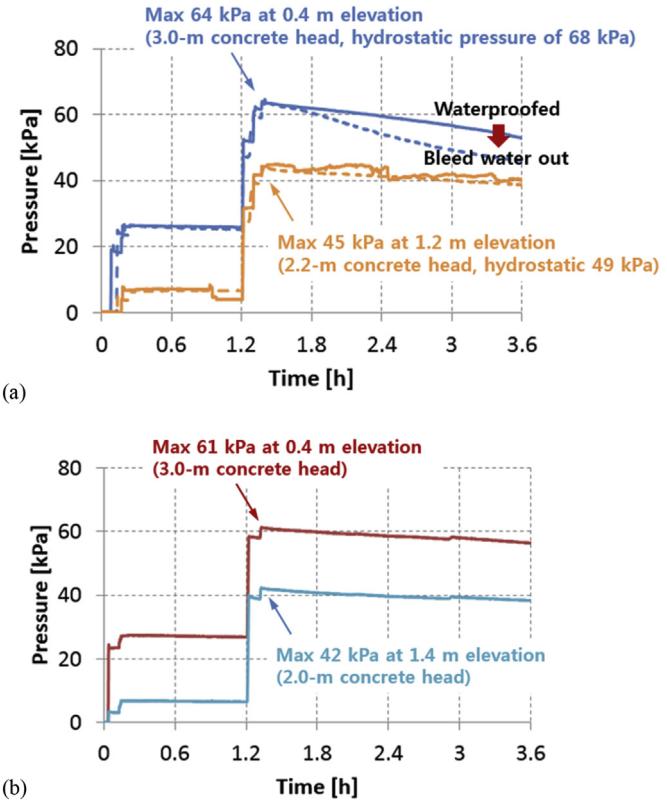

Fig. 3. Mockup test results of (a) NVC0 (solid lines)/NVC2 (dashed lines) and (b) SCC2 (solid lines).

with a piece of Styrofoam, and its connecting part was covered with duct tape. The waterproofed condition on the mounting and connection of the pressure transducers was emphasized. Each pressure transducer was placed at the vertical center line of a form plate. The elevations of the transducers from the bottom of concrete were 0.4 m, 0.8 m, 1.2 m, and 2.1 m, with corresponding concrete heads of 3.0 m, 2.6 m, 2.2 m, or 1.3 m, respectively, after the placement was finished. However, in the case of SCC2 the transducers' elevations were slightly relocated to chase the high pressure at the bottom: 0.4 m, 0.5 m and 1.4 m.

2.2. Mockup test results

Table 3 summarizes the measurement results of the 4 cases, where the form pressure at each elevation is listed. Representative points of the measurements were selected at approximately 0 h, 1 h, and 3 h, which corresponds to the time of initiation, the 2nd-step placement, and 2-h passed. The placement operation made slight variations on the time. Assuming that the form pressure is hydrostatic when the placement has been finished, the pressure level at 3 h indicates the decay of form pressure. Fig. 3 compares the results of 2-step placement: NVC0, a concrete mix showing a 150-mm slump, was placed in a waterproofed form; NVC2, the same mix, was placed on a concrete block; and SCC2, a concrete mix showing a 700-mm slump flow, was placed on a concrete block. As we intended, the forms installed on a concrete block allows the concrete mix to have bleed water out, as shown in Fig. 4. The pictures were taken after 3 h had passed after the NVC mix was completely placed.

Table 3
Representative values of the measurements.

Case	Elevation, m	Pressure at 0 h, kPa	Pressure at 1 h, kPa	Pressure at 3 h, kPa
NVC0	0.4	26	64 (assumed as p_h)	54 (84% p_h)
	0.8	16	53 (assumed as p_h)	48 (91% p_h)
	1.2	6.8	45 (assumed as p_h)	42 (93% p_h)
	2.1	–	24 (assumed as p_h)	22 (92% p_h)
NVC1	0.4	70 (assumed as p_h)	64	48 (69% p_h)
	0.8	67 (assumed as p_h)	63	47 (70% p_h)
	1.2	56 (assumed as p_h)	53	46 (82% p_h)
	2.1	45 (assumed as p_h)	45	42 (93% p_h)
NVC2	0.4	26	64 (assumed as p_h)	47 (72% p_h)
	0.8	16	54 (assumed as p_h)	47 (87% p_h)
	1.2	6.5	45 (assumed as p_h)	39 (87% p_h)
	2.1	–	33 (assumed as p_h)	30 (91% p_h)
SCC2	0.4	27	61 (assumed as p_h)	57 (93% p_h)
	0.5	24	57 (assumed as p_h)	54 (95% p_h)
	1.4	5.7	42 (assumed as p_h)	39 (93% p_h)

[§] The hydrostatic pressure, p_h, is assumed as the form pressure when the placement is finished.

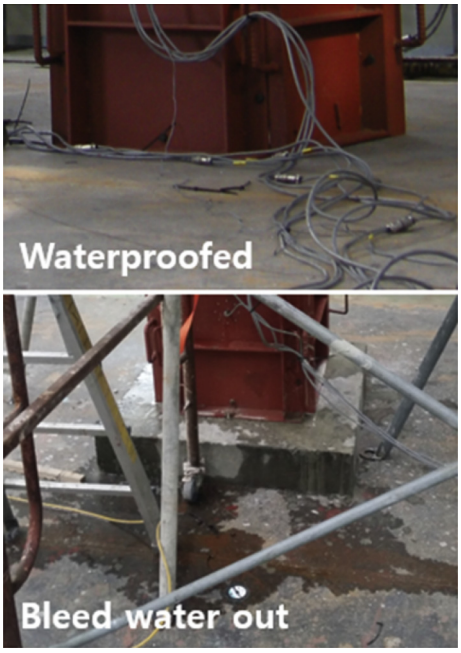

Fig. 4. Comparison of the effect of boundary condition on NVC0 and NVC2.

The effect of bleed water-out (drainage condition) is found in the comparison between the NVC0 and NVC2 cases in Fig. 3 (a). When the 2-step placement was finished at approximately 1.4 h, the form pressures measured at two elevations indicated an almost hydrostatic pressure by the concrete head. At the elevation of 0.4 m, NVC2 case, the drainage condition affected the form pressure from the time of 1.7 h. When the bleed water was allowed to be out of the form, the decrease of its form pressure was steeper than that exerted by the waterproofed form. At the elevation of 1.2 m, the difference according to the drainage condition was not found within the measurement time. Note that at the elevation of 0.8 m, between 0.4 m and 1.2 m, the form pressure on the drainage condition differed from the waterproofed condition later than 1.7 h. In other words, the bleed water-out gradually affects the form pressure from the nearest location of the drainage point (the concrete block). In contrast, the rapid decrease in form pressure of NVC0 (in a waterproofed form) case was not found even though the pressure decay at 0.4 m was slightly faster than the others. Slight water loss might cause the fast decay at the bottommost location (0.4 m) even though the bleed water-out was not observed apparently.

Fig. 3 (b) shows the form pressure exerted by SCC, where the form was installed on a concrete block that allowed the bleed water-out (SCC2). Nevertheless, no bleed water came out because the SCC mix inherently showed little bleeding. Even at the elevation of 0.4 m, denoted by the red line on the figure, only a mild decrease in the form pressure: Approximately −1.4 kPa/h (−3.5% pressure/h) at both elevations of 0.4 m and 1.6 m. The degree of mild decrease was equivalent to that measured at 1.2 m and 2.1 m of the NVC0 case. Therefore, the mild decrease of SCC2 and NVC0 (except for the 0.4 m elevation) is related to the water consumption and air-void compressibility inside a mix. That is the effect of the material itself, which is unaffected by other extrinsic factors such as the bleeding phenomenon. Note that the SCC mix may show external bleeding for a higher column and then rapid decay in the form pressure is expected. The extrinsic effect related to the bleeding phenomenon gets dominant in the situation.

Fig. 5 shows the result of the NVC1 case. Normal concrete was placed at a sitting. At the elevation of 0.4 m, the mild decrease due

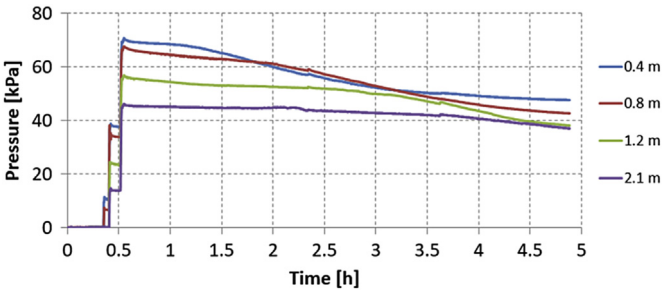

Fig. 5. Mockup test measurement of NVC1 case.

to the intrinsic effect continued until 1.2 h. The rapid decrease started after that time, and it converged to 48 kPa at approximately 4.5 h. The rapid decrease at the elevation of 0.8 m started from 2.0 h and then converged to 43 kPa. The measurement at an upper elevation followed the shifted trend of the sigmoid function form. An effective region in the freshly placed concrete grew tall from the drainage point. The growth of the effective region corresponds with the gradual effect of the bleed water-out from the nearest location of the drainage point (discussed with NVC2 case). The form pressure decreased when a specific elevation was included in the effective region.

2.3. Proof-of-concept test

A small-scale test was designed to verify the effect of the drainage of the bleed water. Control of the waterproofed and bleed water-out conditions are better ensured in a pressure vessel test. Fig. 6 shows the design of the pressure vessel test. The pressure vessel test was variously used to investigate the pressure response of fresh concrete in the study of form pressure [7,8]. Combining the pressure vessel test with the pressurized bleeding test equipment [28–30] allowed us to control the bleed water-out; the bottom nozzle and porous-stone filter on the nozzle were augmented.

A cylindrical sample mixture placed in the pressure vessel with a diameter of 150 mm and a height of 500 mm. The vessel volume was approximately 8.8 L. The bleed water was designed to flow out

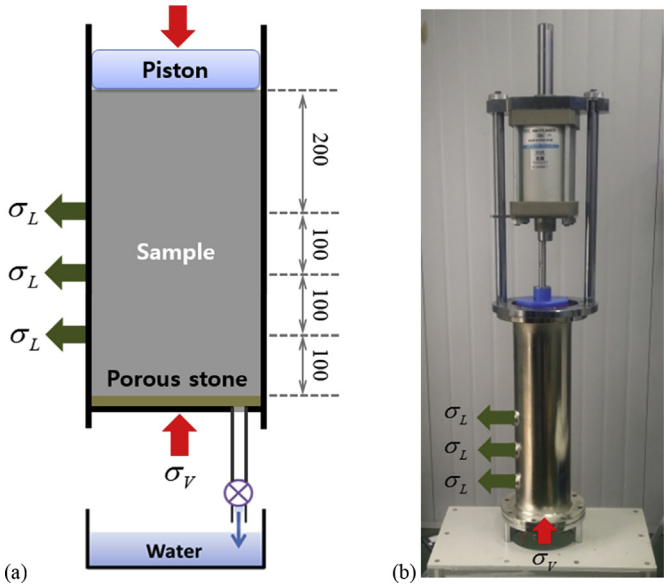

Fig. 6. Pressure vessel for the proof-of-concept test.

to the bottom of the vessel, while the original pressure vessel closed the water drainage in all directions. The vessel was made with 10-mm thick stainless steel, and therefore, no deflection on the vessel was allowed. A porous-stone disc with a 20-μm perforation filtered out the bleed water and allowed to drain to the bottom. No cement particles were found in the drained bleed water. A vertical pressure was applied by the use of a compressed air-cylinder piston system. The piston, the blue piece in the figure, contained 2 rubber O-rings on its circumferential side, which maintained the undrained condition to the upper direction. The top pressure was monitored to control the level of vertical pressure. A load cell having a capacity of 4.9 kN was attached to the loading axis, between the air-cylinder and piston. Dividing the load by the cross-sectional area of the piston provided the top pressure. The bottom pressure was also measured for the evaluation, and this value was used for the vertical pressure (σ_V). The lateral pressure (σ_L) was measured at 3 elevations: 100 mm, 200 mm, and 300 mm from the bottom. For the pressure measurement, the same pressure transducer used for the mockup test was assembled in each socket of the pressure vessel. Fig. 6 (b) shows the picture of the test device.

The proof-of-concept test was accomplished using a mortar sample, which allowed us to have a stable pressure response while excluding coarse aggregates' prodding on the sensor. The water-to-cement ratio of the mortar sample was 0.49 by mass, and its sand-to-cement ratio was 3.3 by mass. The volume fractions of cement and aggregate in the mortar mix were similar to those of the SCC, but the water content increased to compensate for the water absorption of the aggregates (sand). HRWRA, 2.2% dosage per cement content, was also incorporated to provide a slump of 130 mm with no segregation.

First, the waterproof test was performed with only water filling the pressure vessel. The bottom and lateral pressures were measured for the undrained boundary condition. The bottom valve was closed. The applied top pressure was 2.86 bar, and the bottom pressure was measured as 2.46 bar. The difference of 0.4 bar was caused by the friction of the blue piston. The lateral pressure exerted by water was 2.41 bar, which was almost hydrostatic, as expected.

When the mortar sample was placed in the pressure vessel, for the undrained condition, the bottom pressure became 1.97 bar for the same applied top pressure (2.86 bar). The 500-mm high mortar cylinder additionally produced a friction of 0.49 bar. The lateral pressure was 1.97 bar, the same as the vertical (bottom) pressure again. The measurement was continued for 2 h after the sample was casted, during which, the reading of the pressures was constant. Therefore, it can be confirmed that cement-based materials under the undrained condition is in a state of hydrostatic pressure.

For the replicated mortar sample, the pressure vessel test was performed, but with a drained condition. The bottom nozzle was opened to allow bleed water-out. The bleed water filled a beaker in thick drops. After 2 h had passed, during a full measurement, the total bleeding ratio was 5.5%. Only 94.5% of the mixing water remained in the mortar sample at the end. Fig. 7 shows the pressure measurement while the bleeding continued for 2 h, which highlights the rapid decrease of the lateral pressure. The vertical pressure was controlled to ascend stepwise while the bottom pressure was being monitored. The bottom pressure recorded in a data logger increased by 1 bar every 10 min and was kept constant at the highest level of 5 bar. The measured lateral pressure decreases over time. At an elevation of 100 mm, which is the closest to the bottom drainage path, the lateral pressure rapidly dropped and was much lower than the pressure measured at the upper elevations. The further the location from the drainage path, the higher the lateral pressure. The decrease of the lateral pressure asymptotically converged, even though 2 h was too short to identify a converging

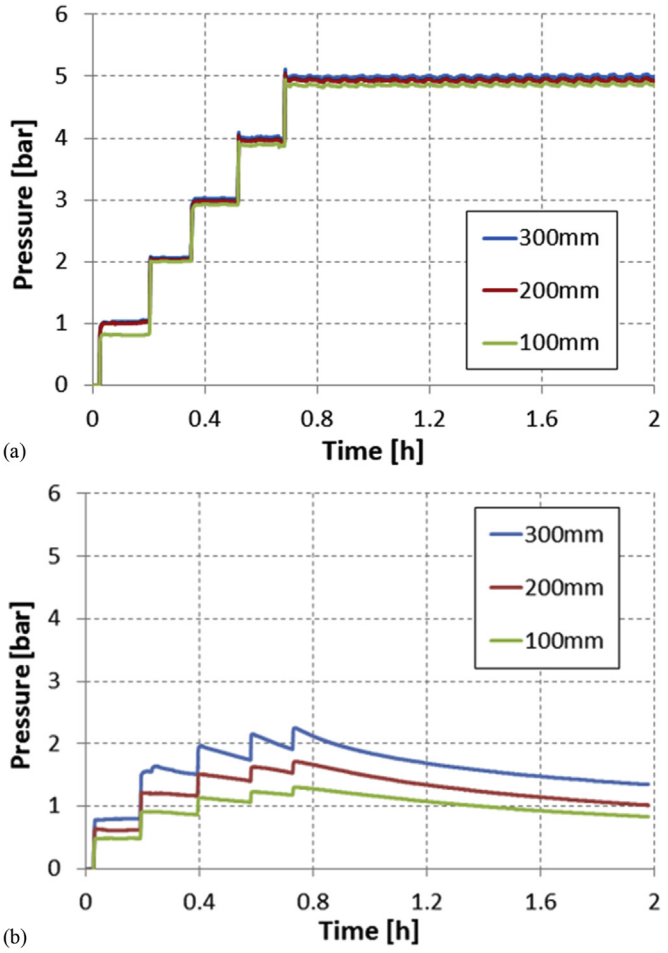

Fig. 7. Measurement of the proof-of-concept test: (a) bottom pressure and (b) lateral pressure.

value. The phenomenon observed in the mockup test, the growth of the effective region, was clearly reproduced in the pressure vessel test.

3. Discussion and modeling

3.1. Formulation of pore pressure diffusion

The effect of bleed water-out can be formulated by the pore pressure diffusion. Biot [31] idealized the pore pressure diffusion in an elastic porous solid, the theory of linear poroelasticity, and developed a constitutive equation:

$$\begin{cases} \sigma_{ij} = \lambda\delta_{ij}\varepsilon_{kk} + 2\mu\varepsilon_{ij} - \zeta\delta_{ij}p \\ \dfrac{m - m_0}{\rho_0} = \dfrac{\zeta}{K}\dfrac{\sigma_{kk}}{3} + \dfrac{\zeta}{KB}p \end{cases}, \tag{1}$$

where σ_{ij} is the Cauchy stress, ε_{ij} is the Green strain, p is the pore fluid pressure and m is the pore fluid mass content. The behavior of the elastic porous solid is represented by the Lamé parameters, λ and μ, under a drained condition. The drained bulk modulus in the equation is then $K = (3\lambda + 2\mu)/3$. The compressibility of the material is expressed by the Biot coefficient $\zeta = 1 - K/K_s$ and the Skempton coefficient $B = (1/K - 1/K_s)/(1/K - 1/K_s - v_0/K_p + v_0/K_f.)$, where $1/K_s$, $1/K_p$, and $1/K_f$ are the compressibility of the solid skeleton, pore space, and pore fluid, respectively. The initial states of v_0 and m_0 are

the approximate porosity and pore fluid mass content of undisturbed material. In addition, ρ_0 is the pore fluid density at atmospheric pressure. Assuming the transport of pore fluid mass follows Darcy's law,

$$\vec{q} = -\rho_0 \frac{\kappa}{\eta} \vec{\nabla} p \tag{2}$$

with a permeability of κ and viscosity of η, it gives the Laplacian equation for the mass conservation of the pore fluid:

$$\vec{\nabla} \cdot \vec{q} + \frac{\partial m}{\partial t} = -\rho_0 \frac{\kappa}{\eta} \nabla^2 p + \frac{\partial m}{\partial t} = 0. \tag{3}$$

Placing the time derivative of the fluid mass content ($\partial m/\partial t$) in the later Eq. (1) into the above equation gives the following field equation,

$$\nabla^2 p = \frac{\zeta \eta}{\kappa} \frac{\partial}{\partial t}\left(\frac{\sigma_{kk}}{3K}\right) + \frac{\zeta \eta}{\kappa} \frac{\partial}{\partial t}\left(\frac{p}{KB}\right). \tag{4}$$

A concrete mix in a sufficiently stiff form, such that no deformation of formwork is allowed, is constrained to the horizontal direction, $\varepsilon_{ij} = 0$, except in the vertical direction denoted by the Z-axis. The volumetric strain is then equal to the vertical strain: $\varepsilon_{kk} = \varepsilon_{zz}$. The former Eq. (1) provides the strain in compliance form: $\varepsilon_{zz} = (\sigma_{zz} + \zeta p)/(\lambda + 2\mu) = (\sigma_{zz} + \zeta p)/M$ as represented by the oedometric modulus $M = \lambda + 2\mu$. The mean stress under the horizontal constraints is again given by the former Eq. (1):

$$\frac{\sigma_{kk}}{3} = K\varepsilon_{kk} - \zeta p = \frac{K}{M}\sigma_{zz} + \left(\frac{K}{M} - 1\right)\zeta p. \tag{5}$$

Applying the above equation to the field Eq. (4) gives

$$\nabla^2 p = \frac{\zeta \eta}{M\kappa} \frac{\partial \sigma_{zz}}{\partial t} + \frac{1}{c} \frac{\partial p}{\partial t}, \tag{6}$$

where $c = (\kappa/\eta)/(\zeta/KB + \zeta^2/M - \zeta^2/K)$ is the diffusivity of the medium. When the vertical load is instantaneously applied, its stress becomes $\sigma_{zz}(z,t) = -\sigma_V H(t)$ with an initial vertical pressure of σ_V and the Heaviside step function of $H(t)$. The time derivative of the equation is then $\partial\sigma_{zz}/\partial t = -\sigma_V \delta(t)$ with the Dirac delta function of $\delta(t)$. At $t = 0$, the Dirac delta function confines an initial condition $p_0 = p(z,t = 0) = \zeta\eta c\sigma_V/M\kappa$. The assumption of incompressible constituents, $B = \zeta = 1$, simplifies the approximate diffusivity to $c = \kappa M/\eta$ and the initial pore pressure to $p_0 = \sigma_V$. The result of the self-weight bleeding test in the previous study [32] supports the incompressible assumption: the bleed water on a concrete mix keeps a constant level during the time of monitoring. The total volume of the concrete mix, including the bleed water-out, keeps constant: uncompressed. The remaining diffusion equation becomes

$$\nabla^2 p(z,t) = \frac{1}{c} \frac{\partial p}{\partial t}. \tag{7}$$

The drainage point defines the boundary condition of $p(z = 0,t) = 0$. Applying the drainage boundary condition gives an ordinary solution for the above diffusion equation:

$$p(z,t) = p_0 \mathrm{erf}\left(\frac{z}{\sqrt{4ct}}\right) = \sigma_V \mathrm{erf}\left(\frac{z}{\sqrt{4ct}}\right). \tag{8}$$

The radial stress on the solid is then given by the former Eq. (1),

$$\sigma_{rr} = \lambda\varepsilon_{zz} - p = \frac{\nu}{1-\nu}\sigma_{zz} - \frac{1-2\nu}{1-\nu}p, \tag{9}$$

where the vertical strain is $\varepsilon_{zz}=(\sigma_{zz} + p)/M$, as previously described. Replacing the radial and axial stress with the horizontal and vertical pressure on the mix gives

$$\sigma_H = \frac{\nu}{1-\nu}\sigma_V + \frac{1-2\nu}{1-\nu}p \tag{10}$$

and

$$K(z,t) = \frac{\sigma_H}{\sigma_V} = \frac{\nu}{1-\nu} + \frac{1-2\nu}{1-\nu}\mathrm{erf}\left(\frac{z}{\sqrt{4ct}}\right), \tag{11}$$

where K is usually called the Janssen parameter, i.e., the lateral-to-vertical pressure ratio [10].

Fig. 8 shows the Janssen parameter over time. When the vertical pressure is instantaneously applied at $t = 0$, the Janssen parameter becomes $K(z,t = 0) = 1$, with $\mathrm{erf}(t = 0) = 1$. The pore pressure diffuses while the vertical pressure is sustained. The lateral pressure consequently decreases over time. If there is no pore pressure diffusion in the mix, e.g., a waterproofed boundary condition, then no decay in the lateral pressure is expected. Increasing the diffusivity corresponds to rapid decay of the Janssen parameter. In the view of the microstructure, higher diffusivity represents the compact and dense microstructure of freshly mixed concrete, where pore pressure diffusion is less likely to occur. The elapse of sufficient time causes the pore pressure to vanish, $p(z,t\to\infty) = 0$ with $\mathrm{erf}(t\to\infty) = 0$, and then, the Janssen parameter approaches to the value of $\nu/(1-\nu)$, that is, the Poisson's effect of an elastic solid subjected to horizontal constraints. The lateral pressure of an elastic solid cylinder is the product of $\nu/(1-\nu)$ and the vertical pressure when it is compressed under restrained horizontal strain.

3.2. Considering the capillary pressure

Capillary pressure develops in freshly mixed concrete at rest, and the pore pressure diffusion is disturbed by the capillary pressure. Fig. 9 illustrates the effect of capillary pressure. The gray left column is the concrete mix, as represented by the previously described model. The blue right column represents the capillary pressure, even though it is located inside the concrete mix in reality. The capillary pressure is hydrostatic, $\gamma_w z$, with the unit weight of water γ_w, under the assumption of its full connection. The hydrostatic state remains unless it allows the drainage of the capillary water. The vertical pressure for a concrete head of z is given by $p = \gamma_c z$ with the unit weight of concrete. The capillary at the corresponding elevation considers an ideal path to the valve of the

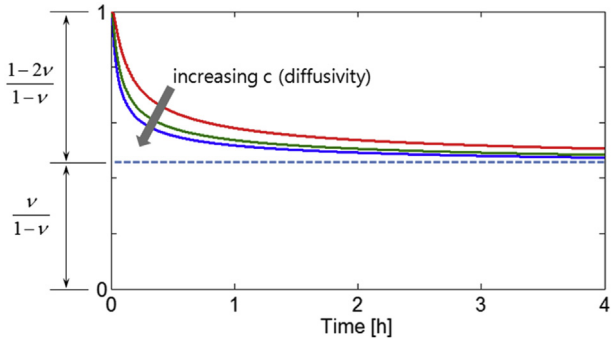

Fig. 8. Decay of Janssen parameter (the value of diffusivity is 3, 6 or 9 mm^2/s).

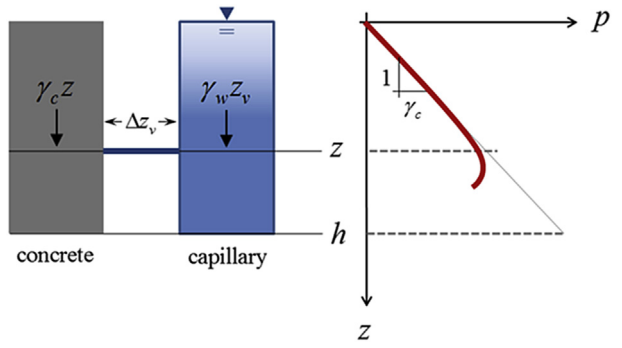

Fig. 9. Effect of capillary pressure.

capillary, which is defined here by the notional diffusing distance (Δz_v). The value of the capillary pressure is then calculated as $p_v = \gamma_w(z + \Delta z_v)$, where γ_w is the unit weight of water. The pressure gradient on the mouth of the capillary is therefore given by

$$\frac{\Delta p_v}{\Delta z_v} = \frac{\gamma_w(z + \Delta z_v) - \gamma_c z}{\Delta z_v}. \tag{12}$$

Applying the pressure gradient on the diffusion equation determines the rate of pore pressure decrease,

$$\frac{\partial p_v}{\partial t} = c\frac{\partial}{\partial z}\left(\frac{\Delta p_v}{\Delta z_v} - \frac{\partial p}{\partial z}\right) = -(\gamma_c - \gamma_w)\frac{c}{\Delta z_v}. \tag{13}$$

The excess pore pressure on the mouth of the capillary begins to dissipate when the capillary opens to a drainage point. The initial hydrostatic pressure in the capillary is released due to the drainage of the capillary water, which becomes bleed water. The capillary pressure gradually decreases from the location of the drainage. The capillary pressure drop at a certain elevation starts only when its capillary pressure is higher than that below its elevation. The effective region observed in the mockup test results is then represented by $p_v(z,t=0) > p_v(z - \Delta z,t)$, where its growth with Δz is incrementally determined by the initial hydrostatic pressure at $t = 0$. No transport of pore water occurs until the above inequality equation is satisfied. The incremental decrease in excess pore pressure in Eq. (13) is then expressed by

$$\Delta p_v(z, t + \Delta t) = -(\gamma_c - \gamma_w)\frac{c}{\Delta z_v}\Delta t \quad \text{if} \quad p_v(z, t=0) > p_v(z - \Delta z, t). \tag{14}$$

The conditional equation for the excess pore pressure addresses the growth of the effective region in the test results. The excess pore pressure diffuses through the capillary, where the capillary is assumed to have a parallel connection on the concrete mix, as shown in Fig. 9. The diffusion of the excess pore pressure is again governed by the diffusion Eq. (7), and its solution in an incremental form is given by

$$\Delta p(z, t + \Delta t) = \Delta p_v(z,t)\,\mathrm{erf}\left(\frac{\Delta z_v}{\sqrt{4c\Delta t}}\right) \text{ if } p_v(z, t=0) > p_v(z - \Delta z, t). \tag{15}$$

However, the pore pressure on the concrete mix diffuses even before the effective region of the drainage arrives at the elevation. The capillary pressure is hydrostatic, and the initial pore pressure of the mix is also hydrostatic due to the unit weight of concrete (γ_c). The two pressures achieve a balance. Therefore, the difference between the two pressures follows the diffusion equation (7), and then, the pore pressure distribution in concrete mix can be evaluated by

$$p(z,t) = \gamma_w z + (\gamma_c z - \gamma_w z)\cdot\mathrm{erf}\left(\frac{\Delta z_v}{\sqrt{4ct}}\right) \quad \text{if} \quad p_v(z, t=0) < p_v(z - \Delta z, t) \tag{16}$$

Finally, replacing Eq. (8) with Eq. (15) or (16) reformulates the form pressure of Eq. (10). Adopting Eq. (15) or Eq. (16) for the pore pressure diffusion is contingent upon the arrival of the effective region.

3.3. Parametric study of the mockup case

Fig. 10 shows the mockup test results of NVC1 and NVC2, where the connected dots are experimental measurements and the solid lines are the estimation using the pore water pressure diffusion model considering the capillary. For the same concrete mix, the material properties were consistently applied for both cases. The unit weight of concrete was $\gamma_c = 24$ kN/m^3 and that of water was $\gamma_c = 9.8$ kN/m^3. The Poisson's ratio of 0.42 taken in the estimation was supposed to describe the behavior of unset concrete. Note that the value is between that of fluid and hardened concrete. The Poisson's ratio of water asymptotically approaches 0.5, and its value for hardened concrete is approximately 0.2. The diffusivity of freshly mixed concrete was set to c = 0.09 m^2/s. The notional diffusing distance was assumed to hold 1.5 times the maximum aggregate size, $\Delta z_v = 1.5 \times 25$ mm $= 37.5$ mm.

The diffusivity is the most important material property related to the water transport through the capillary of a concrete mix, which results in determining the pore water and formwork pressures. It is dependent of the network formation of the capillary and

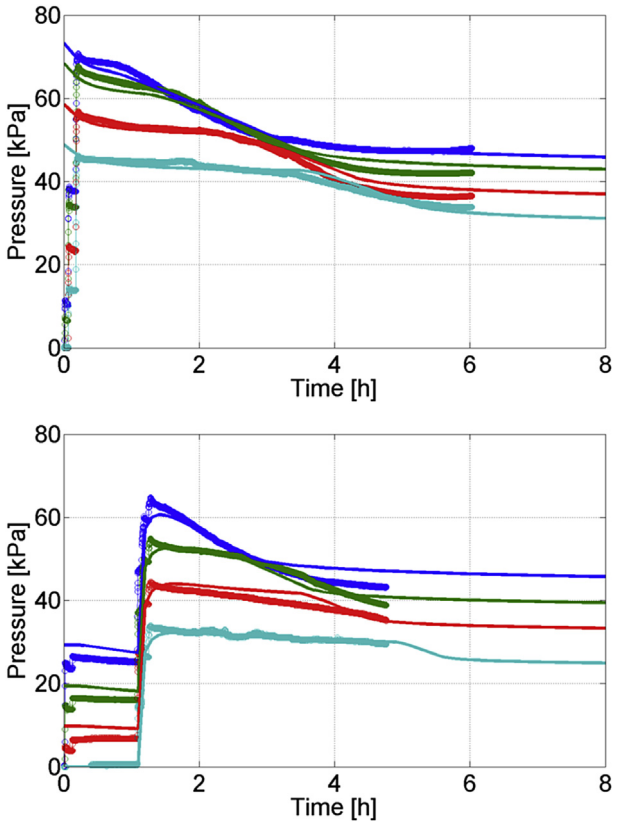

Fig. 10. Model estimation for the mockup test cases: (top) NVC1 and (bottom) NVC2.

the supply of water in the mix. When the authors compare the diffusivity, the estimated value ($c = 0.09\ m^2/s$) is much less than that measured by the pressure vessel-filtration test [21,28,29]. The pressure vessel-filtration test to measure the bleeding under a high pressure gave the diffusivity in the order of 10^{-5}. Therefore, it should be noted that the diffusivity related to the formwork pressure does not have the exactly same with that measured by the pressure vessel-filtration test. Possible factors to make the difference are: (1) mixture compaction by a high pressure level and (2) the supply of free water and interaction with air. The mockup test of the current study was under self-weight and its peak pressure was less than 80 kPa approximately. The pressure vessel-filtration test in references [21,28,29] was performed in a higher level of hydrostatic pressure, and the small-scale samples used for the test would have lack of free water supply and air infiltration. Both factors increase the compactness of the samples, which results in a very low diffusivity.

Considering the form pressure-related diffusivity estimated the lateral pressures of NVC1 and NVC2. For example, the blue line in the NVC1 case is the measurement and estimation at the 0.4-m elevation. The mild decrease of the form pressure until 1.2 h, previously discussed in the test results, is now clarified by balancing the pore water pressure with the capillary pressure, that is, the state before the effective region arrives at the elevation. At a 0.8-m elevation, the balance is disturbed at approximately 2.0 h, which is later than the lower location. The growth of the effective region is driven by the inequality condition of Eq. (16), where the diffusivity of concrete controls the rate of growth. The rapid decrease of lateral pressure was observed only when the bleed water was drained out. The diffusion of the excess pore water pressure in Eq. (14) addresses the rapid decrease. The short distance to the drainage point and 2-dimensional diffusion must be considered for a conventional formwork system, such as a gang form. The lower level of the form pressure is expected for such a conventional formwork condition.

Only the mild decrease of lateral pressure was observed in the measurement exerted by SCC2 (see Fig. 3). The low-diffusivity SCC did not allow bleed water-out, even on the concrete block, and so the drainage condition was not effective. Note that the diffusivity of SCC is reportedly less than that of NVC [33]. The capillary out of the effective region remains hydrostatic, and its balancing with the pore water pressure addresses the mild decrease of the form pressure. The effective region does not evolve in a waterproofed form (NVC0) either, except at the bottommost elevation, for which the state is equivalent to the low-diffusivity SCC mix.

On the other hand, for validating the model parameters, the proposed diffusion model was compared with a conventional model to predict the form pressure. The pressure response model [10,11,34,35] was used for the comparison, because the other thixotropic models [3,4,12–14] predict only the peak formwork pressure exerted by SCC. All models, regardless of their formulating theory, gave comparable results and sufficiently predicted the peak pressure of SCC formwork [36]. The pressure response model distinguishes between instantaneous and delayed responses: $\Delta\sigma_H(\tau,\tau') = \alpha(\tau,\tau')\beta(\tau')\Delta\sigma_V(\tau')$, where τ is the current time and τ' is the time of vertical pressure loading ($\Delta\sigma_V$). Comparing it with the Janssen parameter, in Eq. (11), gives the instantaneous function, $\beta(\tau') \equiv K(z,t = \tau')$, and the delayed function, $\alpha(\tau,\tau') \equiv K(z,t)/\beta(\tau') = K(z,t)/K(z,t = \tau')$. Both functions are then explained with the Poisson's ratio and diffusivity of the proposed model. Fig. 11 shows the single-step pressure response of the NVC1 case, which could be formulated by the Janssen parameter. Considering the pseudo-step function with the rise time of t_0 determined $\beta = 0.6$ and its rate of decrease became $d\alpha/d(\tau - \tau') = 0.1\ h^{-1}$. The rise time ($t_0$) of the pseudo-step presumes a response lag when a sudden increase of vertical pressure is applied in the pressure vessel test for the pressure response model. Both functions are in the range for explaining the form pressure exerted by NVC [10], and they were obviously less than those for general SCC mixes [36].

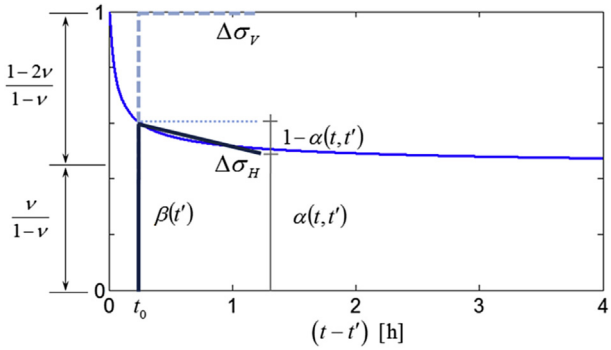

Fig. 11. Comparison between the proposed model and a conventional model.

4. Conclusions

The form pressure exerted by freshly mixed concrete is critical to ensure safety in the construction field. The mechanism of the decay of form pressure is still unclear, even though its design load is presented in a guideline or specification. This paper described a proposal that the diffusion of pore water pressure governs the change of the form pressure. The diffusivity and Poisson's ratio of the unset concrete mix are the material properties in the situation considered. Drainage of bleed water releases the excess pore water pressure, which results in a reduction of the form pressure. A low-diffusivity mix, such as SCC, does not allow bleeding; thus, its form pressure remains almost hydrostatic. The mockup test results, where the form pressure exerted in a waterproofed form is compared with a general case, support the proposed hypothesis. The bleed water of the NVC generally leaks through the joints of the form plates. The pore water pressure diffusion model, considering the capillary pressure proposed in the paper, predicts the lateral pressure decay on the form allowing for bleed water-out. In contrast, NVC in a waterproofed form exerts the hydrostatic pressure that is the same as for SCC.

Acknowledgements

This research was supported by Basic Science Research Program through the National Research Foundation of Korea (NRF) funded by the Ministry of Science, ICT and Future Planning (NRF-2015R1A1A1A05001382).

References

[1] M.K. Hurd, Lateral pressures for formwork design, Concr. Int. (2007) 31–33.
[2] N.J. Gardner, Pressure of concrete on formwork - a review, J. Am. Concr. Inst. 82 (1985) 744–753. <Go to ISI>://WOS: A1985ARX0700020.
[3] C.-A. Graubner, E. Boska, C. Motzko, T. Proske, F. Dehn, Formwork pressure induced by highly flowable concretes - design approach and transfer into practice, Struct. Concr. 13 (2012) 51–60, http://dx.doi.org/10.1002/suco.201100012.
[4] K. Khayat, Effect of section width and casting rate on variations of formwork pressure of self-consolidating concrete, Mater. Struct. 38 (2005) 73–78, http://dx.doi.org/10.1617/14074.
[5] P. Billberg, J. Silfwerbrand, T. Österberg, Form pressures generated by self-consolidating concrete. Casting rate is a dominant factor, Concr. Int. (2005) 35–42. October.
[6] R. McCarthy, J. Silfwerbrand, Comparison of three methods to measure formwork pressure when using SCC field study shows feasible alternatives to predictive methods, Concr. Int. (2011) 27–32.
[7] K.H. Khayat, J.J. Assaad, Measurement systems for determining formwork pressure of highly-flowable concrete, Mater. Struct. 41 (2007) 37–46, http://

dx.doi.org/10.1617/s11527-006-9216-7.
[8] A. Gregori, R.R. Ferron, Z.H. Sun, S.P. Shah, Experimental simulation of self-consolidating concrete formwork pressure, ACI Mater. J. 105 (2008) 97–104. <Go to ISI>://WOS:000253291400012.
[9] S.H. Kwon, S.P. Shah, T.P. Quoc, J.H. Kim, Y. Lee, Intrinsic model to predict formwork pressure, ACI Mater. J. 107 (2010) 20–26. <Go to ISI>://WOS:000274004100003.
[10] J.H. Kim, M.W. Beacraft, S.H. Kwon, S.P. Shah, Simple analytical model for formwork design of self-consolidating concrete, ACI Mater. J. 108 (2011) 38–45. <Go to ISI>://WOS:000286995400005.
[11] J.H. Kim, M. Beacraft, S.P. Shah, Effect of mineral admixtures on formwork pressure of self-consolidating concrete, Cem. Concr. Compos. 32 (2010) 665–671, http://dx.doi.org/10.1016/j.cemconcomp.2010.07.018.
[12] K.H. Khayat, J.J. Assaad, Use of thixotropy-enhancing agent to reduce formwork pressure exerted by self-consolidating concrete, ACI Mater. J. 105 (2008) 88–96. <Go to ISI>://WOS:000253291400011.
[13] K.H. Khayat, J.J. Assaad, Effect of w/cm and high-range water-reducing admixture on formwork pressure and thixotropy of self-consolidating concrete, ACI Mater. J. 103 (2006) 186–193. <Go to ISI>://WOS:000237610900005.
[14] J.J. Assaad, K.H. Khayat, Effect of viscosity-enhancing admixtures on formwork pressure and thixotropy of self-consolidating concrete, ACI Mater. J. 103 (2006) 280–287. <Go to ISI>://WOS:000239330000007.
[15] J. Assaad, K.H. Khayat, Variations of lateral and pore water pressure of self-consolidating concrete at early age, ACI Mater. J. 101 (2004) 310–317.
[16] N.R. Andriamanantsilavo, S. Amziane, Maturation of fresh cement paste within 1- to 10-m-large formworks, Cem. Concr. Res. 34 (2004) 2141–2152, http://dx.doi.org/10.1016/j.cemconres.2004.03.027.
[17] A. Alexandridis, N.J. Gardner, Mechanical-behavior of fresh concrete, Cem. Concr. Res. 11 (1981) 323–339, http://dx.doi.org/10.1016/0008-8846(81)90105-8.
[18] J.J. Assaad, J. Harb, K.H. Khayat, Use of triaxial compression test on mortars to evaluate formwork pressure of self-consolidating concrete, ACI Mater. J. 106 (2009) 439–447. <Go to ISI>://WOS:000270476100005.
[19] G. Ovarlez, N. Roussel, A physical model for the prediction of lateral stress exerted by self-compacting concrete on formwork, Mater. Struct. 39 (2007) 269–279, http://dx.doi.org/10.1617/s11527-005-9052-1.
[20] J.C. Tchamba, S. Amziane, G. Ovarlez, N. Roussel, Lateral stress exerted by fresh cement paste on formwork: laboratory experiments, Cem. Concr. Res. 38 (2008) 459–466, http://dx.doi.org/10.1016/j.cemconres.2007.11.013.
[21] S. Amziane, N. Andriamanantsilavo, Prediction of cement paste pore water pressure variations during setting period, Adv. Cem. Res. 16 (2004) 23–28, http://dx.doi.org/10.1680/adcr.2004.16.1.23.
[22] F.H. Wittmann, On the action of capillary pressure in fresh concrete, Cem. Concr. Res. 6 (1976) 49–56, http://dx.doi.org/10.1016/0008-8846(76)90050-8.
[23] S. Amziane, Setting time determination of cementitious materials based on measurements of the hydraulic pressure variations, Cem. Concr. Res. 36 (2006) 295–304, http://dx.doi.org/10.1016/j.cemconres.2005.06.013.
[24] Y. Vanhove, C. Djelal, A. Magnin, Prediction of the lateral pressure exerted by self-compacting concrete on formwork, Mag. Concr. Res. 56 (2004) 55–62, http://dx.doi.org/10.1680/macr.2004.56.1.55.
[25] S.H. Kwon, Q.T. Phung, H.Y. Park, J.H. Kim, S.P. Shah, Effect of wall friction on variation of formwork pressure over time in self-consolidating concrete, Cem. Concr. Res. 41 (2011) 90–101, http://dx.doi.org/10.1016/j.cemconres.2010.09.009.
[26] M. Arslan, O. Şimşek, S. Subaşı, Effects of formwork surface materials on concrete lateral pressure, Constr. Build. Mater 19 (2005) 319–325, http://dx.doi.org/10.1016/j.conbuildmat.2004.07.007.
[27] S. Amziane, A. Perrot, G. Ovarlez, N. Roussel, SCC formwork pressure: influence of steel rebars, in: K.H. Khayat, D. Feys (Eds.), 6th Int. RILEM Symp. Self-compacting Concr., Montreal, Canada, 2010, pp. 759–771.
[28] H.J. Yim, J.H. Kim, H.-G. Kwak, Experimental simulation of bleeding under a high concrete column, Cem. Concr. Res. 57 (2014) 61–69, http://dx.doi.org/10.1016/j.cemconres.2013.12.011.
[29] V. Picandet, D. Rangeard, A. Perrot, T. Lecompte, Permeability measurement of fresh cement paste, Cem. Concr. Res. 41 (2011) 330–338, http://dx.doi.org/10.1016/j.cemconres.2010.11.019.
[30] A. Perrot, T. Lecompte, H. Khelifi, C. Brumaud, J. Hot, N. Roussel, Yield stress and bleeding of fresh cement pastes, Cem. Concr. Res. 42 (2012) 937–944, http://dx.doi.org/10.1016/j.cemconres.2012.03.015.
[31] M.A. Biot, General theory of three-dimensional consolidation, J. Appl. Phys. 12 (1941) 155, http://dx.doi.org/10.1063/1.1712886.
[32] H.J. Yim, J.H. Kim, H.-G. Kwak, J.K. Kim, Evaluation of internal bleeding in concrete using a self-weight bleeding test, Cem. Concr. Res. 53 (2013) 18–24, http://dx.doi.org/10.1016/j.cemconres.2013.05.015.
[33] J.H. Kim, H.J. Yim, S.H. Kwon, Quantitative measurement of the external and internal bleeding of conventional concrete and SCC, Cem. Concr. Compos 54 (2014) 34–39, http://dx.doi.org/10.1016/j.cemconcomp.2014.05.006.
[34] J.H. Kim, N. Noemi, S.P. Shah, Effect of powder materials on the rheology and formwork pressure of self-consolidating concrete, Cem. Concr. Compos 34 (2012) 746–753, http://dx.doi.org/10.1016/j.cemconcomp.2012.02.016.
[35] S.H. Kwon, J.H. Kim, S.P. Shah, Development and applications of the intrinsic model for formwork pressure of self-consolidating concrete, Int. J. Concr. Struct. Mater 6 (2012) 31–40, http://dx.doi.org/10.1007/s40069-012-0003-2.
[36] M. Alawneh, V. Sekpe, M. Elkady, G. Morcous, R. Scheduler, O. Public, P. District, Comparison of Self Consolidated Concrete Formwork Pressure, 2013, pp. 1–12.